![TU Delft logo]

Delft University of Technology

Selective High-Frequency Mechanical Actuation Driven by the VO$_2$ Electronic Instability

Manca, Nicola; Pellegrino, Luca; Kanki, Teruo; Venstra, Warner J.; Mattoni, Giordano; Higuchi, Yoshiyuki; Tanaka, Hidekazu; Caviglia, Andrea D.; Marré, Daniele

Important note
To cite this publication, please use the final published version (if applicable).
Please check the document version above.

Selective High-Frequency Mechanical Actuation Driven by the VO2 Electronic Instability

Nicola Manca,* Luca Pellegrino, Teruo Kanki, Warner J. Venstra, Giordano Mattoni, Yoshiyuki Higuchi, Hidekazu Tanaka, Andrea D. Caviglia, and Daniele Marré

Relaxation oscillators consist of periodic variations of a physical quantity triggered by a static excitation. They are a typical consequence of nonlinear dynamics and can be observed in a variety of systems. VO2 is a correlated oxide with a solid-state phase transition above room temperature, where both electrical resistance and lattice parameters undergo a drastic change in a narrow temperature range. This strong nonlinear response allows to realize spontaneous electrical oscillations in the megahertz range under a DC voltage bias. These electrical oscillations are employed to set into mechanical resonance a microstructure without the need of any active electronics, with small power consumption and with the possibility to selectively excite specific flexural modes by tuning the value of the DC electrical bias in a range of few hundreds of millivolts. This actuation method is robust and flexible and can be implemented in a variety of autonomous DC-powered devices.

Ultrathin free-standing structures such as membranes or microbridges can efficiently couple their mechanical degrees of freedom to electronic, optical, and magnetic interactions in different excitation/response schemes.[1–4] The use of materials with intrinsic functionalities and complex response to external stimuli constitutes the keystone toward next-generation miniaturized sensors and actuators.[5–8] To this purpose, transition metal oxides are a unique class of materials, where the balance between electronic correlations, magnetic ordering, and lattice distortions gives rise to phase transitions (PTs) and nonlinear behaviors.[9,10] Among them, VO2 is considered a textbook example due to its metal–insulator transition associated with a crystal symmetry change when its temperature is increased above 65 °C.[11] The PT of VO2 is at the same time a puzzling mix of Mott physics, structural distortions,[12–15] and a unique candidate for a variety of technological applications.[16–21] One of the most fascinating characteristics of VO2 is the possibility of realizing a current/voltage periodic instability under constant electrical bias that determines electrical oscillations. Spontaneous oscillations are a hallmark of nonlinear systems,[22] and so far electrical oscillations under DC bias have been observed in several complex oxides characterized by nonlinear current–voltage characteristics.[23–25] In VO2, such unstable state is triggered by the strong nonlinear variation of its electrical properties across the PT. This oscillating state has been investigated in VO2 bulk crystals[26,27] and more recently in single-crystal nanobeams and thin films.[28,29] Several studies showed how it is possible to control the frequency and the onset of this oscillating state either by external parameters, such as device geometry, electrical bias, and laser heating, or by connecting electrical passive elements.[30–33] So far all these studies focused on the analysis of the electrical characteristics of this oscillating state, considering it a potential platform for neural-mimicking computing architectures.[34–37] However, since the PT of VO2 involves both its electronic and lattice properties, electrical oscillations shall also determine strong periodic mechanical forces on the device structure, whose implications have not been studied so far.

Here, we demonstrate how the coupled resistive and structural transition of VO2 can be employed to generate mechanical excitations in the MHz range using only a DC voltage source. This is a local self-actuation mechanism capable of driving the motion of a micromechanical resonator, performing a direct transduction from a voltage bias to high-frequency mechanical excitation, which relies on the intrinsic properties of VO2 only. In contrast to the typical approaches of mechanical actuation,[38–40] our scheme is intrinsic to the device and does not require dedicated driving electronics, reducing device complexity, size, and power consumption.

Dr. N. Manca[+], Dr. W. J. Venstra, G. Mattoni, Prof. A. D. Caviglia
Kavli Institute of Nanoscience
Delft University of Technology
Lorentzweg 1, 2628 CJ Delft, The Netherlands
E-mail: n.manca@tudelft.nl, nicola.manca@spin.cnr.it

Dr. L. Pellegrino, Prof. D. Marré
CNR-SPIN
Corso Perrone 24, 16152 Genova, Italy

Prof. T. Kanki, Y. Higuchi, Prof. H. Tanaka
Institute of Scientific and Industrial Research
Osaka University
Ibaraki, Osaka 567-0047, Japan

Dr. W. J. Venstra
Quantified Air
Lorentzweg 1
Delft 2628 CJ, The Netherlands

Prof. D. Marré
Physics Department
University of Genova
Via Dodecaneso 33, 16146 Genova, Italy

[+]Present Address: Physics Department, University of Genova, Via Dodecaneso 33, 16146 Genova, Italy

(iD) The ORCID identification number(s) for the author(s) of this article can be found under https://doi.org/10.1002/adma.201701618.

DOI: 10.1002/adma.201701618

ADVANCED
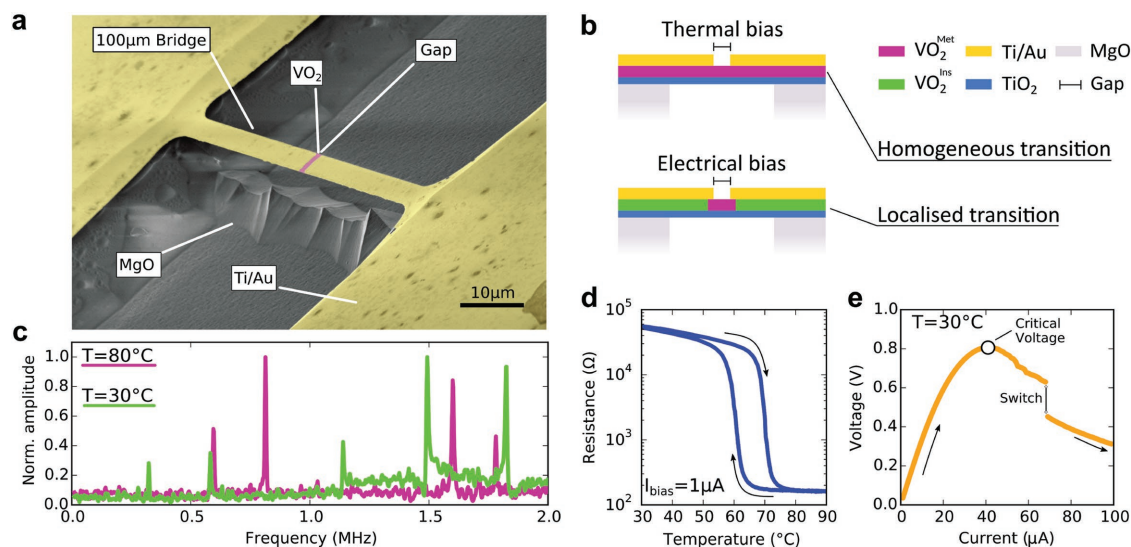**SCIENCE NEWS**
www.advancedsciencenews.com

ADVANCED
MATERIALS
www.advmat.de

Figure 1. Device structure and characterization. a) False-colored scanning electron microscopy picture of a microbridge showing the MgO substrate, the Ti/Au electrodes, and the 2 μm gap of exposed VO$_2$. b) Schematic side view of the microbridge heterostructure illustrating the homogeneous phase transition when the temperature is varied using an external heater (top) and the localized phase transition due to the confined Joule heating (bottom). c) Mechanical response of the microbridge at $T = 30$ °C and $T = 80$ °C taken at 10^{-4} mbar background pressure as measured with an optical detector. A distinct upward shift of the resonance frequencies is detected in the high-temperature phase. d) Resistance versus temperature characteristics of the microbridge taken at low current bias. e) Voltage versus current characteristics of the microbridge. The "Critical Voltage" indicates the point of electrothermal runaway if under voltage bias, while "Switch" indicates the localized phase transition to the metallic state of the VO$_2$ within the gap.

Our device is a 100 μm × 5 μm free-standing microbridge made of a 113 nm thick TiO$_2$/VO$_2$ crystalline bilayer. Metallic Ti/Au electrodes (50 nm thick) partially cover the structure and provide good electrical contact (**Figure 1**a). The TiO$_2$/VO$_2$ heterostructure is deposited by pulsed laser deposition as described in the Experimental Section. The resulting lattice is c-oriented with crystalline domains having orthogonal in-plane orientations.[18,41,42] Details of the fabrication process can be found in the Experimental Section and Section I of the Supporting Information, while further aspects of the device are discussed in Section II (Supporting Information). The PT of VO$_2$ is triggered above 65 °C, where its electrical resistivity drops by more than two orders of magnitude (insulator–to–metal transition) and the lattice symmetry changes from monoclinic to rutile (structural transition). Both effects are observed in the microbridge when it is homogeneously heated by an external thermal bias (Figure 1b, top): the full bridge undergoes the PT, the lattice transformation causes a frequency shift of the mechanical modes up to 50% (Figure 1c and Section III (Supporting Information)), and the electrical resistance shows its characteristic hysteresis loops (Figure 1d). This frequency shift is due to the different in-plane lattice constants of VO$_2$ between the monoclinic and rutile phases,[12] which result in an isotropic strain of 0.08% in the planar directions (Section IV of the Supporting Information), a value much higher than what can be achieved in standard bimetallic strips (bimorph) based on thermal expansion mismatch for the same temperature increase.[43] As a consequence, the device experiences the stress-stiffening[44] and geometric-stiffening[45] effects, where the first is related to an increase of the tension within the structure and the second is a geometric deformation, both increasing the structure rigidity. This wide variation of the internal mechanical stress across the PT has been recently exploited to realize tunable

microelectromechanical systems (MEMS), like programmable resonators and static actuators.[46–51] We note that the mechanical spectra of the microresonator, reported in Figure 1c, differ from that of the simple double-clamped beam model. This is because, as discussed in Section II (Supporting Information), the device profile has a slightly buckled shape due to the built-in compressive stress within the heterostructure. In Section V (Supporting Information), we show finite element simulations of the mechanical modes of our microbridge under buckling conditions and how strain can determine the measured frequency shifts.

In order to excite the resonator without altering its mechanical spectrum, we designed Ti/Au electrodes on top of the free-standing structure that leave a small active VO$_2$ region just within their gap, as indicated in Figure 1a. Since the electrical and thermal resistivity of gold are negligible compared to VO$_2$, these electrodes localize the voltage drop on the VO$_2$ gap only and enhance its thermal contact with the clamped region. An electrical bias applied to the microbridge thus results in heating by Joule effect which is localized in the VO$_2$ gap, eventually triggering its PT. Here, the metal electrodes play the crucial role of limiting the spread of the VO$_2$ metallic phase (Figure 1b, bottom), making the mechanical spectrum independent from the electrical current (see Section III in the Supporting Information). The voltage–current relationship $V(I)$ of the microbridge is plotted in Figure 1e, showing how the characteristic features given by VO$_2$ are retained. The nonmonotonic behavior with a negative differential resistance observed above 40 μA and the sharp jump at 60 μA are the key elements for the realization of electrical oscillations, as will be discussed below.

A consequence of the nonlinear $V(I)$ of VO$_2$ is the onset of electrical oscillations under DC bias. This state has been obtained using the circuit of **Figure 2**a, where a DC voltage

**ADVANCED
SCIENCE NEWS**

www.advancedsciencenews.com

**ADVANCED
MATERIALS**

www.advmat.de
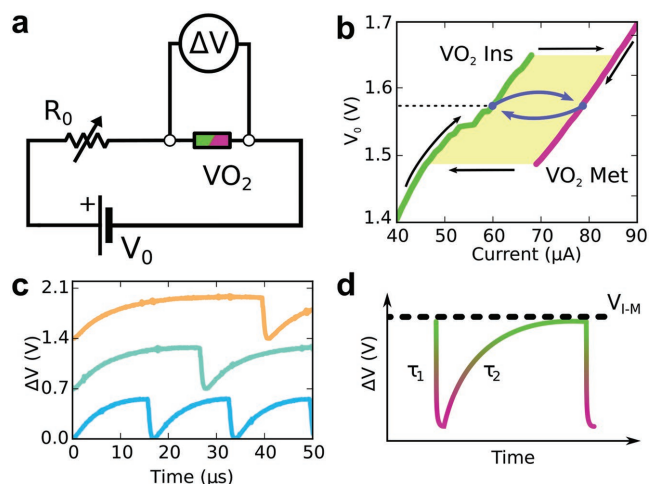
Figure 2. Electrical oscillations under DC bias. a) Electrical circuit used to characterize the electrical oscillation. V_0 is the applied DC voltage, and R_0 is the variable load resistor. b) Voltage–current characteristic of the circuit in (a), with $R_0 = 15$ kΩ. The Joule effect triggers the PT of VO$_2$, resulting in a hysteresis loop (black arrows). The yellow region indicates the voltage range where multiple current values are allowed. Under voltage bias (dashed line), specific combinations of V_0 and R_0 make the system oscillating, with a continuous switching between the two states (blue arrows). c) Tuning of the oscillation period by varying R_0 for $V_0 = 1.5$ V. From top to bottom: 16.25 kΩ (orange), 13.75 kΩ (green), 10 kΩ (blue). Traces are shifted by 0.7 V for clarity. d) The time constants of the two half periods, t_1 and t_2, are given by the different relaxation times of the metallic and insulating states, respectively. The switching from insulating to metallic state is triggered when the voltage drop across the VO$_2$ gap reaches a critical value ($V_{I-M} = 0.6$ V), which also depends on the device geometry.

source (V_0) is applied to the VO$_2$ microbridge and to a load resistor (R_0). Their total voltage–current characteristic is reported in Figure 2b and illustrates the origin of the electrical oscillations in the circuit. By sweeping the current magnitude, it is possible to track the hysteresis in the $V(I)$ relationship due to the PT in the VO$_2$. At around 70 μA, the VO$_2$ switches from insulating (green) to metallic (magenta) state, with lower electrical resistance. When the circuit of Figure 2a is biased with a DC voltage, the hysteresis window determines a range of values where two current conditions are allowed (yellow region). Under a constant voltage bias (dashed line), the voltage drop across the microbridge depends on the metallic or insulating state of VO$_2$. In the insulating state, the voltage is localized across the microbridge by choosing the values of R_0 well below the electrical resistance of the VO$_2$ element. The resulting temperature increase can trigger the PT, lowering the microbridge electrical resistance. In this case, the voltage drop is mainly across the load resistor and the Joule heating on the microbridge is reduced, the temperature decreases, and the initial insulating state is recovered starting a new cycle. This continuous switching is a relaxation-oscillation condition[22] and is triggered for specific combinations of R_0 and V_0.[52] Figure 2c shows the voltage drop across the microbridge as a function of time, while the electrical oscillations are triggered for $V_0 = 1.5$ V and different R_0 between 10 and 20 kΩ. These electrical oscillations have a double-exponential wave shape (Figure 2d), where the time constants τ_1 and τ_2 of the semiperiods are determined by the thermal and electrical RC constants of the system. Their
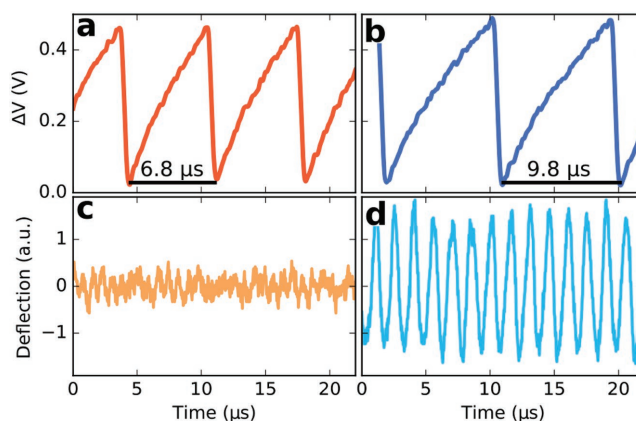

Figure 3. Coupling electrical oscillation to mechanical motion. a,b) Time-domain electrical oscillations measured for two different periods of the electrical relaxation oscillation are shown. c,d) The corresponding deflection signal measured at the same time by the photodiode is shown. The trace in (c) has small amplitude and no clear harmonic component, while panel (d) shows that, for specific values of f_{EO}, a strong periodic signal is detected. These traces were acquired by keeping a constant $V_0 = 2$ V and R_0 in the 10–20 kΩ range.

amplitude is constant and is determined by the critical voltage for the insulator-to-metal transition of the VO$_2$ element (V_{I-M} of Figure 2d). The electrical oscillation frequency (f_{EO}), instead, can be controlled from 20 to 150 kHz by adjusting R_0 and V_0.

By tuning f_{EO}, it is possible to excite the mechanical motion of the microbridge. This is detected by measuring the deflection of the device with an optical lever setup, while the DC circuit is set to trigger the electrical oscillations (see Section VI in the Supporting Information). **Figure 3** shows the time plots of the voltage drop measured across the microbridge (panels a, b) and its corresponding mechanical deflection (panels c, d) while the electrical oscillations are present. For a generic combination of R_0 and V_0, the mechanical motion has small amplitude and no dominant harmonic component (panels a, c). However, for specific values of these parameters, and consequently specific f_{EO}, a strong harmonic mechanical response is observed at frequencies much higher than the electrical one (panels b, d). This response corresponds to a mechanical resonance of the microbridge as measured in Figure 1c, meaning that, for specific f_{EO} values, the low-frequency electrical oscillations trigger resonant motion of the microbridge well above f_{EO}. As discussed in the next section, this is possible because the relaxation oscillation is nonsinusoidal and thus containing harmonic components at higher frequencies.

The coupled electronic and structural transition of VO$_2$ makes possible three parallel mechanisms to achieve mechanical actuation: actuation by structural transition, actuation by thermal expansion, and electrostatic coupling. The first mechanism comes from the VO$_2$ lattice change during the PT, where the unit cell periodically expands and contracts when switching between the insulating/monoclinic and metallic/rutile phases. Thermal excitation comes from the Joule heating produced by the oscillating current, which results in a periodic thermal expansion of the structure. The electrostatic actuation originates from the periodic oscillation of the microbridge voltage with respect to ground, which produces a net capacitive force
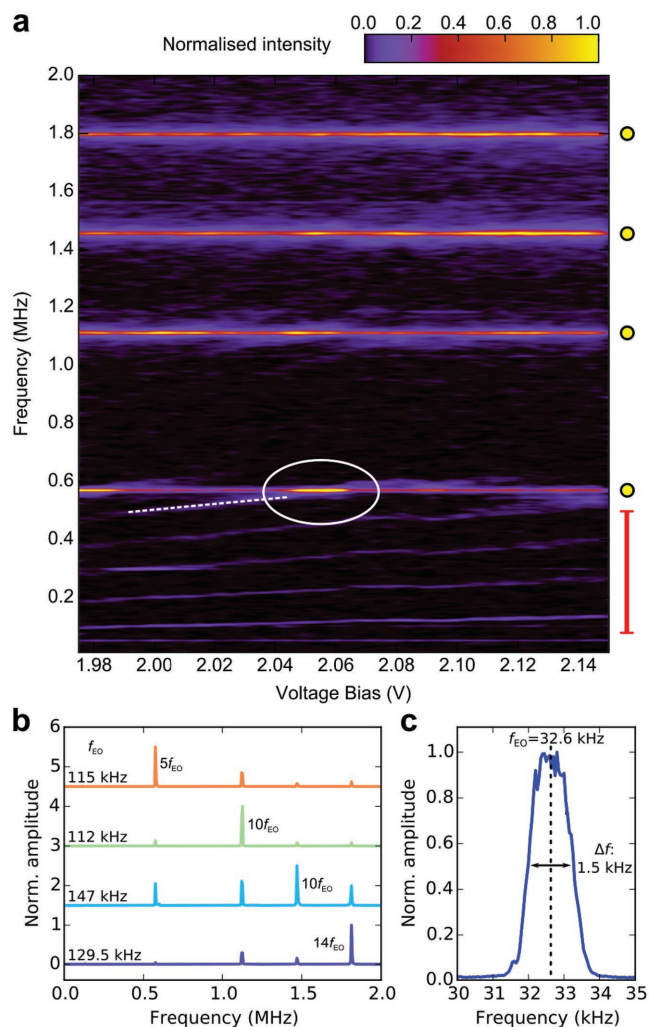
Figure 4. Selective excitation of the mechanical resonance modes. a) Color map showing the selective excitation of different mechanical modes of the microbridge by voltage bias: R_0 is fixed at 20 kΩ while V_0 is varied. Resonant mechanical excitation is obtained when a harmonic component of the electrical oscillations matches a mechanical eigenfrequency of the microbridge (yellow dots). b) Power spectral density of the photodiode signal taken at four different f_{EO} values. The amplitude of a specific mode is enhanced when its frequency (575, 1120, 1470, and 1800 kHz) matches with one of the higher harmonics of the electrical signal. The harmonic number is indicated in the figure. c) Frequency jitter of the electrical oscillation, measured by averaging 100 spectra acquired over 40 s.

coupled to the surrounding dielectric environment. All these three components are periodically modulated by the VO$_2$ PT, and can contribute synergistically to the mechanical actuation with a periodic excitation at f_{EO} and at its higher harmonics. An evaluation of their magnitude is presented in Section VII (Supporting Information).

We now demonstrate how the excitation of the different mechanical modes of the microbridge can be controlled by the electrical bias. **Figure 4**a shows the power spectra of the deflection of the device measured by the photodiode as a function of V_0, and with fixed $R_0 = 20$ kΩ. In this configuration, V_0 controls the relaxation-oscillation frequency f_{EO}, making our device

a voltage-controlled electrical oscillator with a gain of about 250 kHz V^{-1}. In Figure 4a, a comb of dim peaks is visible at low frequencies, marked with the red bar. This is an off-resonance response of the device, corresponding to the first few harmonics of the electrical signal of Figure 2c. By tuning V_0, it is possible to match the frequency of one of these harmonic components with a flexural mode of the microbridge (yellow circles). This condition is realized, for example, at the crossing point indicated by the white oval in Figure 4a, where the increase of amplitude of the specific flexural mode is obtained through resonant excitation by the fifth harmonic of the electrical signal, also visible as forced mechanical oscillation in the unmatched condition (white dashed line). The selective excitation of different mechanical modes is achieved by tuning f_{EO} to obtain the desired matching condition, as shown in the spectra of Figure 4b. The labels indicate the matched harmonic component (nf_{EO}) and the frequency of the selected mode, where, as an example, the 575 kHz peak is excited with the fifth harmonic component of $f_{EO} = 115$ kHz.

An important characteristic of an oscillator is its frequency stability. In our device, the selectivity of the different mechanical modes is determined by the stability of the electrical oscillation. Figure 4c shows an average of 100 acquisitions of the electrical oscillations spectra taken over 40 s for $f_{EO} = 32.6$ kHz. Its width indicates that the amplitude of the frequency jitter of the electrical oscillations, i.e., their stability over time, is about 4–5%. This means that even in an unmatched condition, fluctuations of f_{EO} can trigger the resonant actuation of modes close to one of its harmonic components. This explains why in Figure 4a,b the mechanical modes of the microbridge are slightly visible also in the unmatched condition: as the integration time of the network analyzer is much longer than these fluctuations, the instrument shows the averaged mechanical response. The magnitude of the frequency jitter is related to the robustness of the two switching conditions of the VO$_2$ within the gap and may be improved by optimizing device design, growth methods, or metal contacts.

In this last paragraph, we evaluate the energy efficiency of our device, how it scales with the size of the active region, and compare the presented approach with other actuation mechanisms based on self-oscillation in micro- and nano-structures. The total amount of energy provided to the system is the total Joule power P_{tot} dissipated in the circuit of Figure 2a while the electrothermal oscillations are activated. It can be evaluated by considering that the $V(I)$ characteristic of the circuit in Figure 2b has upper limit: $P_{tot} = V_0 \cdot I_{EO} = (1.6 \text{ V}) \cdot (80 \text{ }\mu\text{A}) = 130 \text{ }\mu\text{W}$. Since the load resistor is comparable to the gap resistance in the insulating phase,[52] as a first approximation, this power is evenly split between the microbridge and R_0. The power required to undergo a periodic PT of a VO$_2$ volume (V) is the product between frequency and heat absorbed by the transition: $P_{PT}/V = f_{EO}(\Delta T c_{p,VO2} + \lambda_{VO2})\rho_{VO2}$, where $\rho_{VO2} = 4.6$ g cm^{-3} is the VO$_2$ density, $\lambda = 51$ J g^{-1} is the latent heat of the transition, and $c_{p,VO2} = 0.75$ J K^{-1} g^{-1} is the VO$_2$ specific heat.[53,54] For a frequency of 100 kHz, a temperature variation of 10 K, and a volume corresponding to the VO$_2$ gap, the resulting average power is about $P_{PT} = 24$ μW. This value is well below the actual power dissipated in the microbridge, meaning that the power consumption of our device is dominated by thermal

dissipations. Several reports in literature discuss the energy efficiency and performances of VO_2-based static and quasi-static actuators.[55–57] Here, it is relevant to compare the device power consumption with other self-actuation mechanisms proposed so far. In suspended membranes of 2D materials, for example, it is possible to trigger self-oscillations by focusing a diverging beam of laser light.[58] However, in order to achieve the light flux gradients required to trigger a resonant excitation, several mW of power (>2 mW) are needed. Furthermore, scaling is limited by diffraction, complex optics are necessary, and the actuation is not mode-selective. A different approach relies on a self-biasing feedback loop, typically coupled with an electrostatic actuator.[38,59,60] In this case, the power consumption is dominated by the active electronic components in the feedback circuits. Here, a single amplifying element, as reported in the datasheets of the components used in the experiments, requires at least 1 W of electrical power. In this context, the total power consumption of our VO_2-based mechanical actuation mechanism is dramatically lower. Also, since it depends on the volume of VO_2 undergoing the PT, it scales with the device size, thus foreseeing an enhanced efficiency for nanoscale devices. Efficient VO_2-based NEMS oscillators could also be employed as actuators for other mechanical resonators. In this picture, the VO_2 would work similarly to a piezoelectric element, but with the added benefit of a direct DC–AC transduction. In this case, the mechanical modes of the VO_2 device could be set to work far from its mechanical resonances, while f_{EO} should match the modes of the target structure by introducing additional passive electrical elements in the circuit of Figure 2a.

In conclusion, we realized a simple and flexible actuation scheme for high-frequency mechanical resonators based on a phase-change material. The intrinsic physical properties of VO_2 allow the direct conversion of a small DC voltage into a mechanical excitation in the MHz range without the need of an external driving circuit. This device can be viewed as a spontaneous voltage-controlled oscillator, which is able to selectively excite the different mechanical modes of a microstructure by controlling the bias voltage. Our actuation mechanism can be implemented in a variety of MEMS requiring resonant actuation, and the device size can be scaled down to comprise just a single sub-micrometric VO_2 domain, allowing individual actuation of nanometric structures. Furthermore, the use of VO_2 single-crystal nanobeams may offer improved performances thanks to the steeper resistive transition and the highly ordered lattice structure. Our approach is scalable both in size and number of devices, where multiple micro-/nanoresonators can be actuated in parallel by a single DC source. This opens the possibility of realizing DC-powered arrays of microactuators, fast frequency-switching devices or sensors based on multifrequency detection, with potential applications spanning from microrobotics to microfluidic devices and environmental monitoring.

Experimental Section

Device Fabrication: The TiO_2 (23 nm)/VO_2 (90 nm) heterostructure is grown on top of a MgO (100) single-crystal substrate by Pulsed Laser Deposition. During the growth, the substrate temperature was kept at 450 °C and the laser fluency was 18 mJ cm^{-2}. TiO_2 is deposited in 0.1 Pa of O_2 with a laser repetition rate of 3 Hz, while VO_2 in 0.95 Pa of O_2 with a repetition rate of 2 Hz. The device is patterned by e-beam lithography using Poly(methyl-methacrylate) resist. Ti (5 nm)/Au (45 nm) electrodes are deposited by electron beam evaporation, followed by lift-off in acetone. The bridge geometry is defined by Ar ion milling with an energy of 500 eV and an ion flux of about 0.2 mA cm^{-1}. The structures are suspended by selective etching of the MgO substrate in H_3PO_4 (8.5% aqueous solution).

Detecting Mechanical Motion: Microbridge motion is detected with a focused laser by an optical lever technique. The laser wavelength is 658 nm and the focused spot size about 2–3 μm, well within the bridge width. The spot is focused at about one fourth of the bridge length, guaranteeing the maximum geometric gain of the optical lever. The laser power is kept low in order to minimize additional heating effects. This is checked before each measurement by monitoring the electrical resistance of the microbridge with and without the laser on the structure. The device is placed in a vacuum chamber with a Peltier element and a Pt100 thermometer. Sample temperature is controlled with a PID feedback loop and kept fixed at 30 °C unless indicated otherwise. All the mechanical spectra have been measured at 10^{-4} mbar. The mechanical spectrum of Figure 1c is measured using a Vector Network Analyzer through thermal excitation, by sending a small AC current of $I_0(1 + \sin(\omega t))$, $I_0 = 5$ μA. This current value is well below that needed to drive the PT of VO_2 in the microbridge.

Reported Data: Measurements reported in Figures 3 and 4 have been acquired from different microbridges fabricated on the same sample. Measurements reported in Figure 4a,b have been acquired in different runs. In Figure 4a, a dim peak is visible at about 50 kHz whose frequency is voltage independent. This signal is due to electronic interference in the photodiode preamplifier and does not affect the measurements. The mechanical power spectra of Figure 4a are measured using a spectrum analyzer from the signal from the photodiode while the electrical oscillations are present. The average of 20 traces is shown, where each trace contains 801 data points, taken across a frequency span of 10 kHz–2 MHz, with a measurement bandwidth of 1 kHz.

Supporting Information

Supporting Information is available from the Wiley Online Library or from the author.

Acknowledgements

Conflict of Interest

The authors declare no conflict of interest.

Keywords

[1] J. S. Bunch, A. M. van der Zande, S. S. Verbridge, I. W. Frank, D. M. Tanenbaum, J. M. Parpia, H. G. Craighead, P. L. McEuen, *Science* **2007**, *315*, 490.

[2] D. Van Thourhout, J. Roels, *Nat. Photonics* **2010**, *4*, 211.

[3] R. Riedinger, S. Hong, R. A. Norte, J. A. Slater, J. Shang, A. G. Krause, V. Anant, M. Aspelmeyer, S. Gröblacher, *Nature* **2016**, *530*, 313.

[4] A. Castellanos-Gomez, V. Singh, H. S. J. van der Zant, G. A. Steele, *Ann. Phys.* **2015**, *527*, 27.

[5] S. C. Masmanidis, R. B. Karabalin, I. de Vlaminck, G. Borghs, M. R. Freeman, M. L. Roukes, *Science* **2007**, *317*, 780.

[6] J. Park, H. Qin, M. Scalf, R. T. Hilger, M. S. Westphall, L. M. Smith, R. H. Blick, *Nano Lett.* **2011**, *11*, 3681.

[7] W. H. Grover, A. K. Bryan, M. Diez-Silva, S. Suresh, J. M. Higgins, S. R. Manalis, *Proc. Natl. Acad. Sci. USA* **2011**, *108*, 10992.

[8] Y. Tao, J. M. Boss, B. a Moores, C. L. Degen, *Nat. Commun.* **2014**, *5*, 3638.

[9] M. Imada, A. Fujimori, Y. Tokura, *Rev. Mod. Phys.* **1998**, *70*, 1039.

[10] E. Morosan, D. Natelson, A. H. Nevidomskyy, Q. Si, *Adv. Mater.* **2012**, *24*, 4896.

[11] F. J. Morin, *Phys. Rev. Lett.* **1959**, *3*, 34.

[12] V. Eyert, *Ann. Phys.* **2002**, *11*, 650.

[13] J. D. Budai, J. Hong, M. E. Manley, E. D. Specht, C. W. Li, J. Z. Tischler, D. L. Abernathy, A. H. Said, B. M. Leu, L. A. Boatner, R. J. McQueeney, O. Delaire, *Nature* **2014**, *515*, 535.

[14] J. S. Brockman, L. Gao, B. Hughes, C. T. Rettner, M. G. Samant, K. P. Roche, S. S. P. Parkin, *Nat. Nanotechnol.* **2014**, *9*, 453.

[15] S. Kumar, J. P. Strachan, M. D. Pickett, A. Bratkovsky, Y. Nishi, R. S. Williams, *Adv. Mater.* **2014**, *26*, 7505.

[16] T. Driscoll, H.-T. Kim, B.-G. Chae, B.-J. Kim, Y.-W. Lee, N. M. Jokerst, S. Palit, D. R. Smith, M. Di Ventra, D. N. Basov, *Science* **2009**, *325*, 1518.

[17] M. a. Kats, R. Blanchard, S. Zhang, P. Genevet, C. Ko, S. Ramanathan, F. Capasso, *Phys. Rev. X* **2013**, *3*, 41004.

[18] L. Pellegrino, N. Manca, T. Kanki, H. Tanaka, M. Biasotti, E. Bellingeri, A. S. Siri, D. Marré, *Adv. Mater.* **2012**, *24*, 2929.

[19] N. Shukla, A. V. Thathachary, A. Agrawal, H. Paik, A. Aziz, D. G. Schlom, S. K. Gupta, R. Engel-Herbert, S. Datta, *Nat. Commun.* **2015**, *6*, 7812.

[20] L. Xiao, H. Ma, J. Liu, W. Zhao, Y. Jia, Q. Zhao, K. Liu, Y. Wu, Y. Wei, S. Fan, K. Jiang, *Nano Lett.* **2015**, *15*, 8365.

[21] H. Yoon, M. Choi, T. W. Lim, H. Kwon, K. Ihm, J. K. Kim, S.-Y. Y. Choi, J. Son, *Nat. Mater.* **2016**, *15*, 1113.

[22] A. Jenkins, *Phys. Rep.* **2013**, *525*, 167.

[23] M. D. Pickett, J. Borghetti, J. J. Yang, G. Medeiros-Ribeiro, R. S. Williams, *Adv. Mater.* **2011**, *23*, 1730.

[24] T. C. Jackson, A. A. Sharma, J. A. Bain, J. A. Weldon, L. Pileggi, *IEEE J. Emerging Sel. Top. Circuits Syst.* **2015**, *5*, 230.

[25] X. Liu, S. Li, S. K. Nandi, D. K. Venkatachalam, R. G. Elliman, *J. Appl. Phys.* **2016**, *120*, 124102.

[26] Y. Taketa, F. Kato, M. Nitta, M. Haradome, *Appl. Phys. Lett.* **1975**, *27*, 212.

[27] B. Fisher, *J. Appl. Phys.* **1978**, *49*, 5339.

[28] Q. Gu, A. Falk, J. Wu, L. Ouyang, H. Park, *Nano Lett.* **2007**, *7*, 363.

[29] Y. W. Lee, B. J. Kim, J. W. Lim, S. J. Yun, S. Choi, B. G. Chae, G. Kim, H. T. Kim, *Appl. Phys. Lett.* **2008**, *92*, 162903.

[30] H.-T. Kim, B.-J. Kim, S. Choi, B.-G. Chae, Y. W. Lee, T. Driscoll, M. M. Qazilbash, D. N. Basov, *J. Appl. Phys.* **2010**, *107*, 23702.

[31] G. Seo, B.-J. Kim, Y. W. Lee, S. Choi, J.-H. Shin, H.-T. Kim, *Thin Solid Films* **2011**, *519*, 3383.

[32] B.-J. Kim, G. Seo, J. Choi, H.-T. Kim, Y. W. Lee, *Jpn. J. Appl. Phys.* **2012**, *51*, 107302.

[33] Y. Wang, J. Chai, S. Wang, L. Qi, Y. Yang, Y. Xu, H. Tanaka, Y. Wu, *J. Appl. Phys.* **2015**, *117*, 64502.

[34] S. Datta, N. Shukla, M. Cotter, A. Parihar, A. Raychowdhury, *Proc. 51st Annual Design Automation Conf. — DAC'14*, ACM Press, New York, USA, **2014**, p. 1.

[35] N. Shukla, A. Parihar, E. Freeman, H. Paik, G. Stone, V. Narayanan, H. Wen, Z. Cai, V. Gopalan, R. Engel-Herbert, D. G. Schlom, A. Raychowdhury, S. Datta, *Sci. Rep.* **2014**, *4*, 4964.

[36] A. Beaumont, J. Leroy, J. C. Orlianges, A. Crunteanu, *J. Appl. Phys.* **2014**, *115*, https://doi.org/10.1063/1.4871543.

[37] A. Pergament, A. Crunteanu, A. Beaumont, G. Stefanovich, A. Velichko, *ArXiv* **2016**, 9.

[38] X. L. Feng, C. J. White, A. Hajimiri, M. L. Roukes, *Nat. Nanotechnol.* **2008**, *3*, 342.

[39] Q. P. Unterreithmeier, E. M. Weig, J. P. Kotthaus, *Nature* **2009**, *458*, 1001.

[40] S. H. Baek, J. Park, D. M. Kim, V. A. Aksyuk, R. R. Das, S. D. Bu, D. a. Felker, J. Lettieri, V. Vaithyanathan, S. S. N. Bharadwaja, N. Bassiri-Gharb, Y. B. Chen, H. P. Sun, C. M. Folkman, H. W. Jang, D. J. Kreft, S. K. Streiffer, R. Ramesh, X. Q. Pan, S. Trolier-McKinstry, D. G. Schlom, M. S. Rzchowski, R. H. Blick, C. B. Eom, *Science* **2011**, *334*, 958.

[41] K. Okimura, T. Furumi, *Jpn. J. Appl. Phys.* **2005**, *44*, 3192.

[42] Y. Muraoka, Z. Hiroi, *Appl. Phys. Lett.* **2002**, *80*, 583.

[43] J. Cao, W. Fan, Q. Zhou, E. Sheu, A. Liu, R. C. Barrett, J. Wu, *J. Appl. Phys.* **2010**, *108*, 83538.

[44] R. B. Karabalin, L. G. Villanueva, M. H. Matheny, J. E. Sader, M. L. Roukes, *Phys. Rev. Lett.* **2012**, *108*, 1.

[45] V. Pini, J. J. Ruz, P. M. Kosaka, O. Malvar, M. Calleja, J. Tamayo, *Sci. Rep.* **2016**, *6*, 29627.

[46] A. Rua, F. Fernàndez, N. Sepúlveda, *J. Appl. Phys.* **2010**, *107*, 74506.

[47] H. Wang, W. He, G. Yuan, X. Wang, Q. Chen, *Thin Solid Films* **2013**, *540*, 168.

[48] N. Manca, L. Pellegrino, T. Kanki, S. Yamasaki, H. Tanaka, A. S. Siri, D. Marré, *Adv. Mater.* **2013**, *25*, 6430.

[49] K. Liu, C. Cheng, J. Suh, R. Tang-Kong, D. Fu, S. Lee, J. Zhou, L. O. Chua, J. Wu, *Adv. Mater.* **2014**, *26*, 1746.

[50] E. Merced, D. Torres, X. Tan, N. Sepulveda, *J. Microelectromech. Syst.* **2015**, *24*, 100.

[51] H. Ma, J. Hou, X. Wang, J. Zhang, Z. Yuan, L. Xiao, Y. Wei, S. Fan, K. Jiang, K. Liu, *Nano Lett.* **2017**, *17*, 421.

[52] P. Maffezzoni, L. Daniel, N. Shukla, S. Datta, A. Raychowdhury, *IEEE Trans. Circuits Syst.* **2015**, *62*, 2207.

[53] J. Cao, E. Ertekin, V. Srinivasan, W. Fan, S. Huang, H. Zheng, J. W. L. Yim, D. R. Khanal, D. F. Ogletree, J. C. Grossman, J. Wu, *Nat. Nanotechnol.* **2009**, *4*, 732.

[54] C. N. Berglund, H. J. Guggenheim, *Phys. Rev.* **1969**, *185*, 1022.

[55] K. Wang, C. Cheng, E. Cardona, J. Guan, K. Liu, J. Wu, *ACS Nano* **2013**, *7*, 2266.

[56] H. Guo, K. Wang, Y. Deng, Y. Oh, S. A. Syed Asif, O. L. Warren, Z. W. Shan, J. Wu, A. M. Minor, *Appl. Phys. Lett.* **2013**, *102*, 231909.

[57] R. Cabrera, E. Merced, N. Sepulveda, *J. Microelectromech. Syst.* **2014**, *23*, 243.

[58] R. A. Barton, I. R. Storch, V. P. Adiga, R. Sakakibara, B. R. Cipriany, B. Ilic, S. P. Wang, P. Ong, P. L. McEuen, J. M. Parpia, H. G. Craighead, *Nano Lett.* **2012**, *12*, 4681.

[59] C. Chen, S. Lee, V. V Deshpande, G.-H. Lee, M. Lekas, K. Shepard, J. Hone, *Nat. Nanotechnol.* **2013**, *8*, 923.

[60] C. Chen, D. H. Zanette, J. R. Guest, D. A. Czaplewski, D. López, *Phys. Rev. Lett.* **2016**, *117*, 17203.